Expanded View Figures

Figure EV1. METTL3 but not WTAP protects METTL14 protein.

A RT-qPCR analysis of the expression levels of *METTL3* and *METTL14* in siRNA knockdown *METTL3* cells. Data are mean ± SEM of three biological replicates and were analyzed by two-tailed unpaired *t*-test. ***$P < 0.001$; n.s., not significant.

B Immunoblots showing total METTL3 protein levels in FLAG-tagged *METTL3*-overexpressing cells. β-actin was used as the loading control. The total METTL3/β-actin densitometric ratio was recorded by ImageJ.

C Immunoblots showing METTL14 and WTAP protein levels in *WTAP* knockdown cells. β-actin was used as the loading control. The METTL14 or WTAP/β-actin densitometric ratio was recorded by ImageJ.

D Immunoblots showing METTL14 protein levels in FLAG-tagged METTL3 or HA-tagged *WTAP*-overexpressing cells. β-actin was used as the loading control. The METTL14/ β-actin densitometric ratio was recorded by ImageJ.

Source data are available online for this figure.

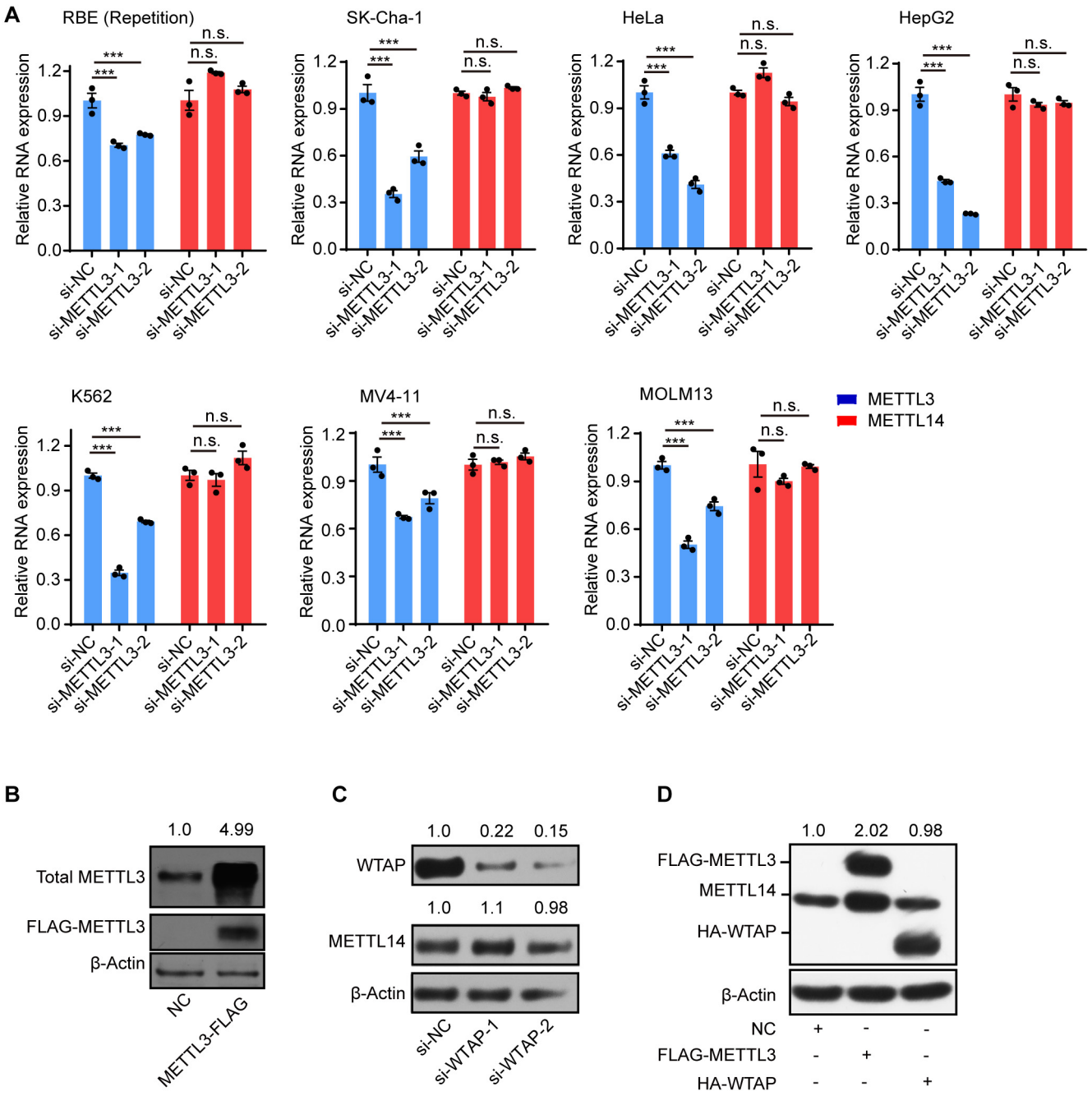

Figure EV1.

Figure EV2. STUB1 interacts with METTL14 but is dispensable for regulating *METTL14* mRNA levels.

A List of the "Proteasome" category in the METTL14 interactome identified by MS, including five PSMAs, one PSMBs, four PSMCs, and eight PSMDs.

B Immunoblots showing PSMD3-myc protein levels in myc-tagged *PSMD3*- overexpressing cells. β-actin was used as the loading control.

C RT-qPCR analysis of the efficiency of shRNA-knockdown for *STUB1*, *UBR1*, *UBR5*, and *TRIM33*. *β-actin* was used as the reference. Data are mean ± SEM of three biological replicates and were analyzed by two-tailed unpaired *t*-test. (n.s., not significant; ***$P < 0.001$).

D, E Co-IP of METTL14 and STUB1 in HEK293T and SK-Cha-1 cells.

F RT-qPCR analysis of expression levels of *STUB1* and *METTL14* in *STUB1* knockdown cells. Data are mean ± SEM of three biological replicates and were analyzed by two-tailed unpaired *t*-test. ***$P < 0.001$; n.s., not significant.

Source data are available online for this figure.

A

Protein ID	METTL14 unique peptide	NC unique peptide	Description
METTL3	38	NA	N6-adenosine-methyltransferase 70 kDa subunit
METTL14	35	NA	N6-adenosine-methyltransferase subunit
PSMD1	9	NA	26S proteasome non-ATPase regulatory subunit 1
PSMD3	7	NA	26S proteasome non-ATPase regulatory subunit 3
PSMC5	5	NA	26S protease regulatory subunit 8
PSMC2	6	NA	26S protease regulatory subunit 7
PSMA4	4	NA	Proteasome subunit alpha type-4
PSMD6	4	NA	26S proteasome non-ATPase regulatory subunit 6
PSMC1	2	NA	26S protease regulatory subunit 4
PSMD12	3	NA	26S proteasome non-ATPase regulatory subunit 12
PSMD13	2	NA	26S proteasome non-ATPase regulatory subunit 13
PSMA3	2	NA	Proteasome subunit alpha type-3
PSMA7	2	NA	Proteasome subunit alpha type-7
PSMA8	2	NA	Proteasome subunit alpha type-7-like
PSMC6	1	NA	26S protease regulatory subunit 10B
PSMD4	1	NA	26S proteasome non-ATPase regulatory subunit 4
PSMB3	1	NA	Proteasome subunit beta type-3
PSMA6	1	NA	Proteasome subunit alpha type-6

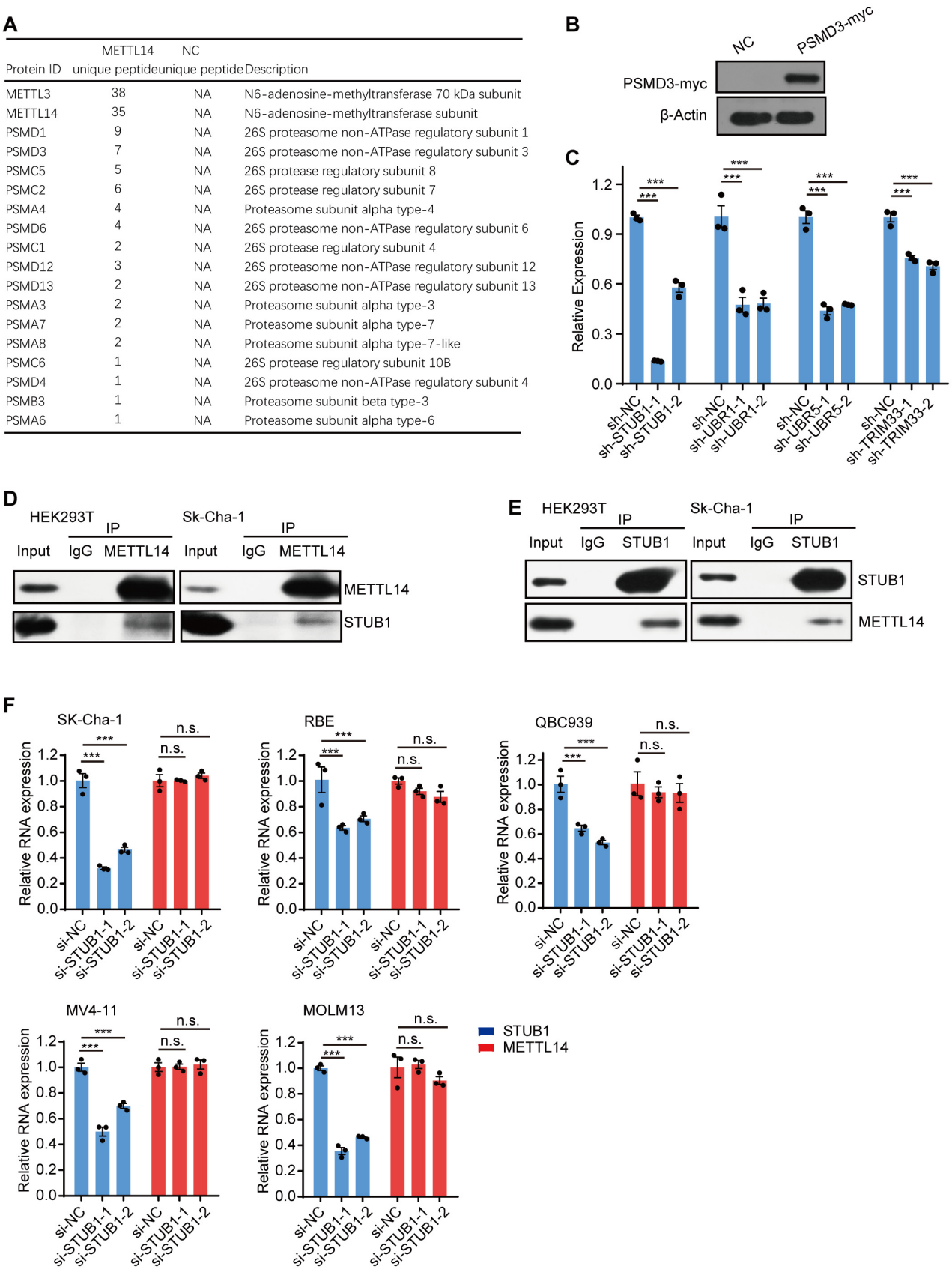

Figure EV2.

Figure EV3. Possible ubiquitination sites in METTL14.

A Schematic diagram of METTL14-domain-deletion mutants. All mutants were GFP-tagged.
B Co-IP of GFP-tagged METTL14-domain-deletion mutant with FLAG-tagged STUB1.
C Immunoblots showing purified GST-STUB1-His, STUB1-His, GST-METTL14, and METTL14.
D Dot blot assays showing the role of sh-*STUB1* in regulating m^6A levels.
E Schematic diagram of the lysine sites located at aa 111–285 of METTL14.
F METTL14 ubiquitination, as detected by IP of a series of lysine (K)-to-arginine (R) mutations in aa 111–285. The accumulation of Ub and METTL14 was confirmed in whole-cell lysates. WT, wild type.

Source data are available online for this figure.

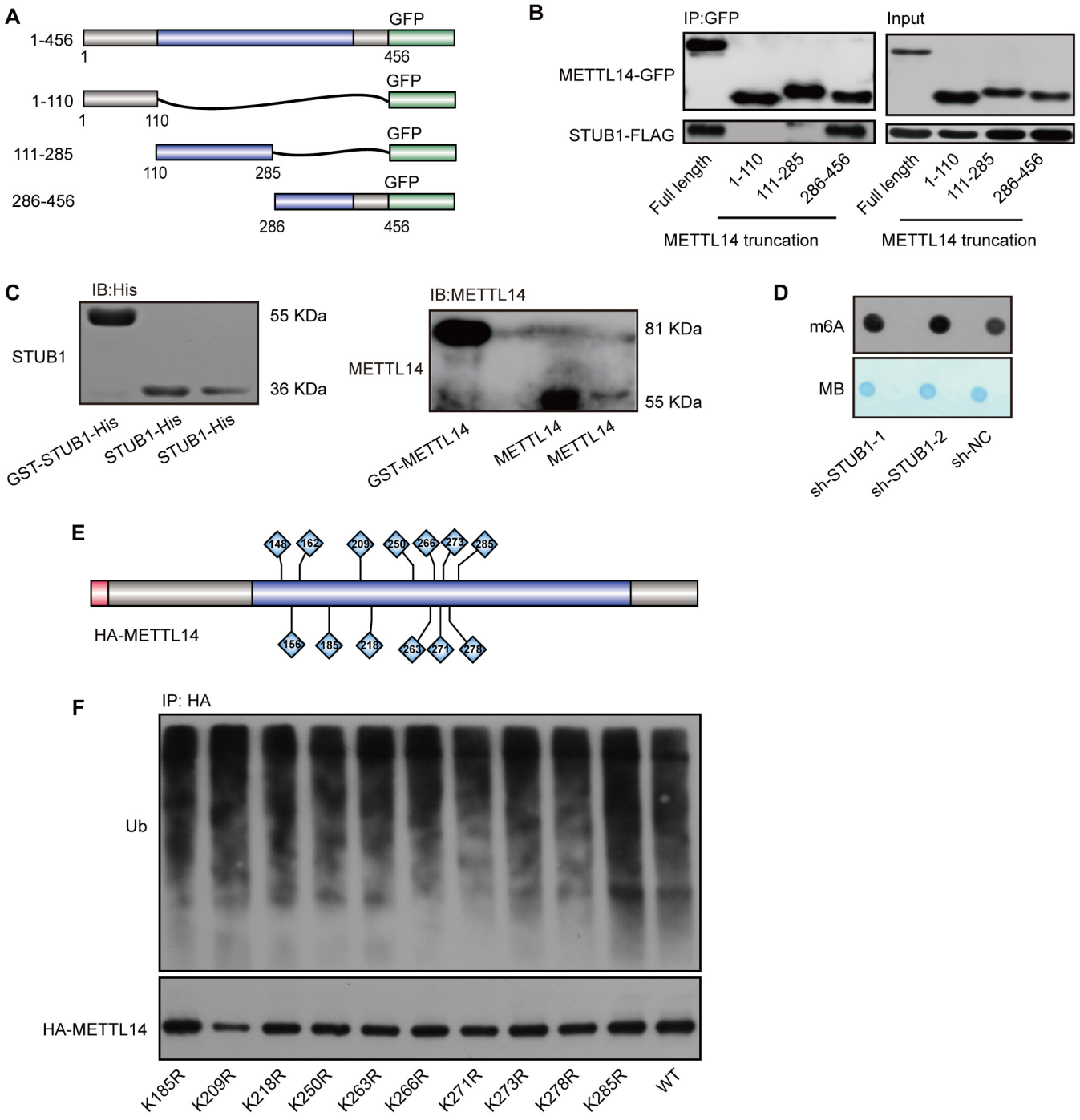

Figure EV3.

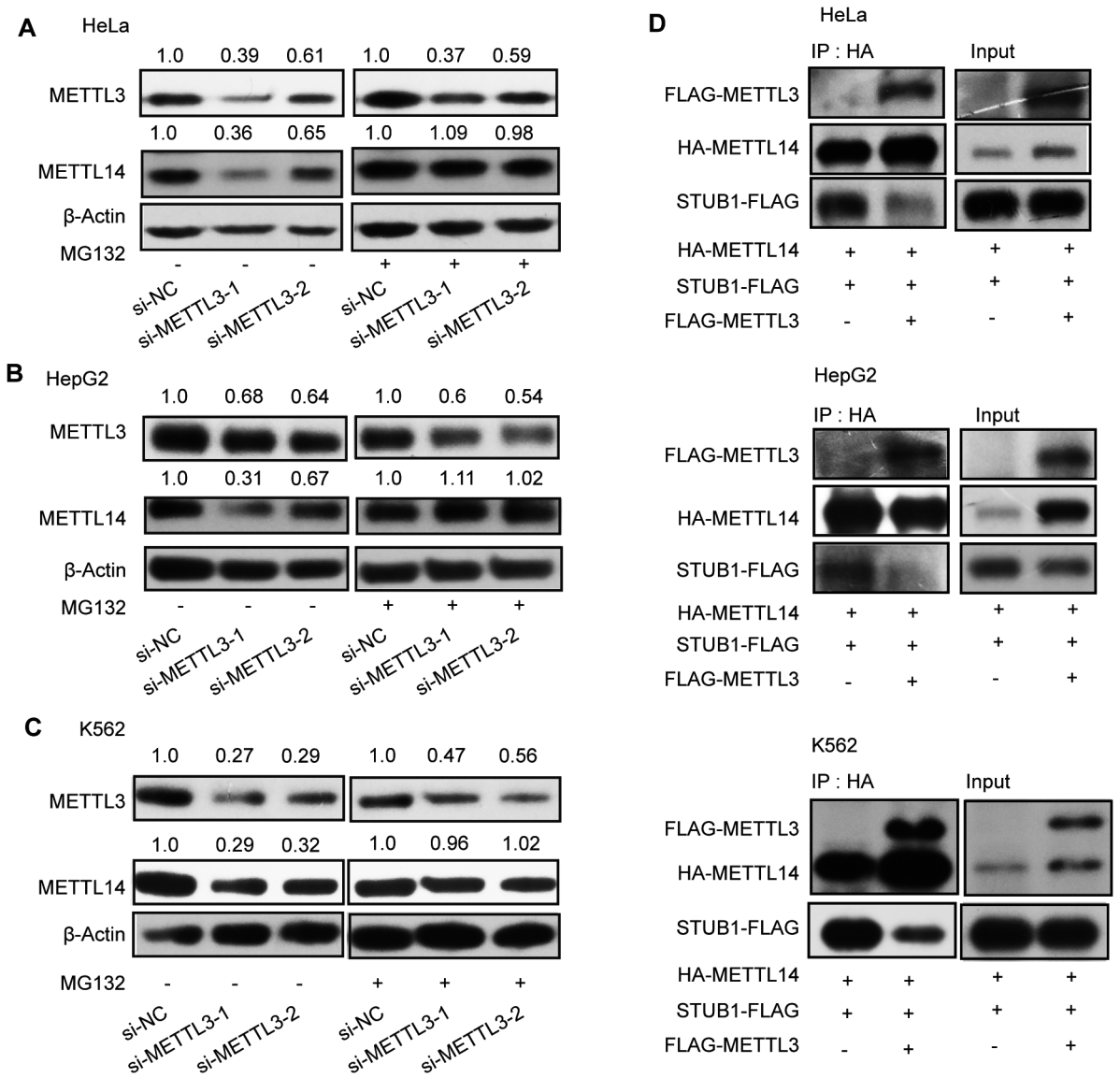

Figure EV4. METTL3 protects METTL14 from STUB1-mediated ubiquitination.

A–C Immunoblots showing METTL14 protein levels under *METTL3* knockdown with or without 10 μM MG132 treatment in HeLa (A), HepG2 (B), and K562 (C) cells. β-actin was used as the loading control. The METTL3 or METTL14/β-actin densitometric ratio was recorded by ImageJ.

D Immunoblots showing the interaction between METTL14 and STUB1 detected by IP with or without FLAG-METTL3 in HeLa, HepG2, and K562 cells.

Source data are available online for this figure.

Figure EV5. STUB1-mediated degradation of METTL14 can suppress CCA progression and has potential clinical relevance.

A Morphology of colonies of Sk-Cha-1 cells upon shRNA-mediated *STUB1* knockdown. Data are mean ± SEM of three biological replicates and were analyzed by two-tailed unpaired *t*-test. (***P* < 0.01).

B CCK-8 assays showing cell viability after shRNA-mediated *STUB1* knockdown. Data are mean ± SEM of three biological replicates and were analyzed by two-way ANOVA. (***P* < 0.01).

C Immunoblots showing METTL14 protein levels in CCA cells overexpressing *STUB1-FLAG*. β-actin was used as the loading control. The METTL14 /β-actin densitometric ratio was recorded by ImageJ.

D CCK-8 assays showing cell viability in MZ-Cha-1 cells overexpressing *STUB1*. Data are mean ± SEM of three biological replicates and were analyzed by two-way ANOVA (****P* < 0.001).

E Immunoblots showing METTL14 protein levels under *STUB1* knockdown and *METTL14* knockdown (left panel) in RBE cells. β-actin was used as the loading control. The METTL14 or STUB1/β-actin densitometric ratio was recorded by ImageJ. CCK-8 assays showing cell viability upon the function of METTL14 in *STUB1* knockdown cells (right panel). Data are mean ± SEM of three biological replicates and were analyzed by two-way ANOVA (****P* < 0.001).

F–H Following the subcutaneous inoculation of SK-Cha-1-sh-NC (left) and SK-Cha-1-sh-*STUB1-2* (right) cells into the flanks of male nude mice (F), *STUB1* knockdown promoted the proliferation of malignant cells (G) and increased subsequent tumor size and growth (H). Data are mean ± SEM. Statistical significance was analyzed by two-way ANOVA (G) and two-tailed unpaired *t*-test (H) (Six mice, **P* < 0.05; ***P* < 0.01).

I Pan-cancer analysis using TGCA data sets consisting of 1,210 patient samples showing that *METTL14* and *STUB1* expression is negatively correlated (Pearson's correlation coefficient − 0.3443, *P* < 0.001).

J Immunoblot analysis showing METTL3 and METTL14 protein levels in eight pairs of CCA patient samples. N, adjacent non-tumor tissue; T, tumor tissue. GAPDH was used as the loading control. The METTL3 or METTL14 /GAPDH densitometric ratio was recorded by ImageJ.

K–M STUB1 protein levels are low in patient samples with high carcinoembryonic antigen and total bilirubin, and intrahepatic metastasis in the Fudan University intrahepatic cholangiocarcinoma (FU-iCCA) cohort (using patient samples from the 5–95% bin according to STUB1 protein levels; a two-tailed unpaired *t*-test was used). In the boxplot, the central band indicates the median, the box indicates the interquartile range, and the whiskers indicate the 5–95% percentile.

Source data are available online for this figure.

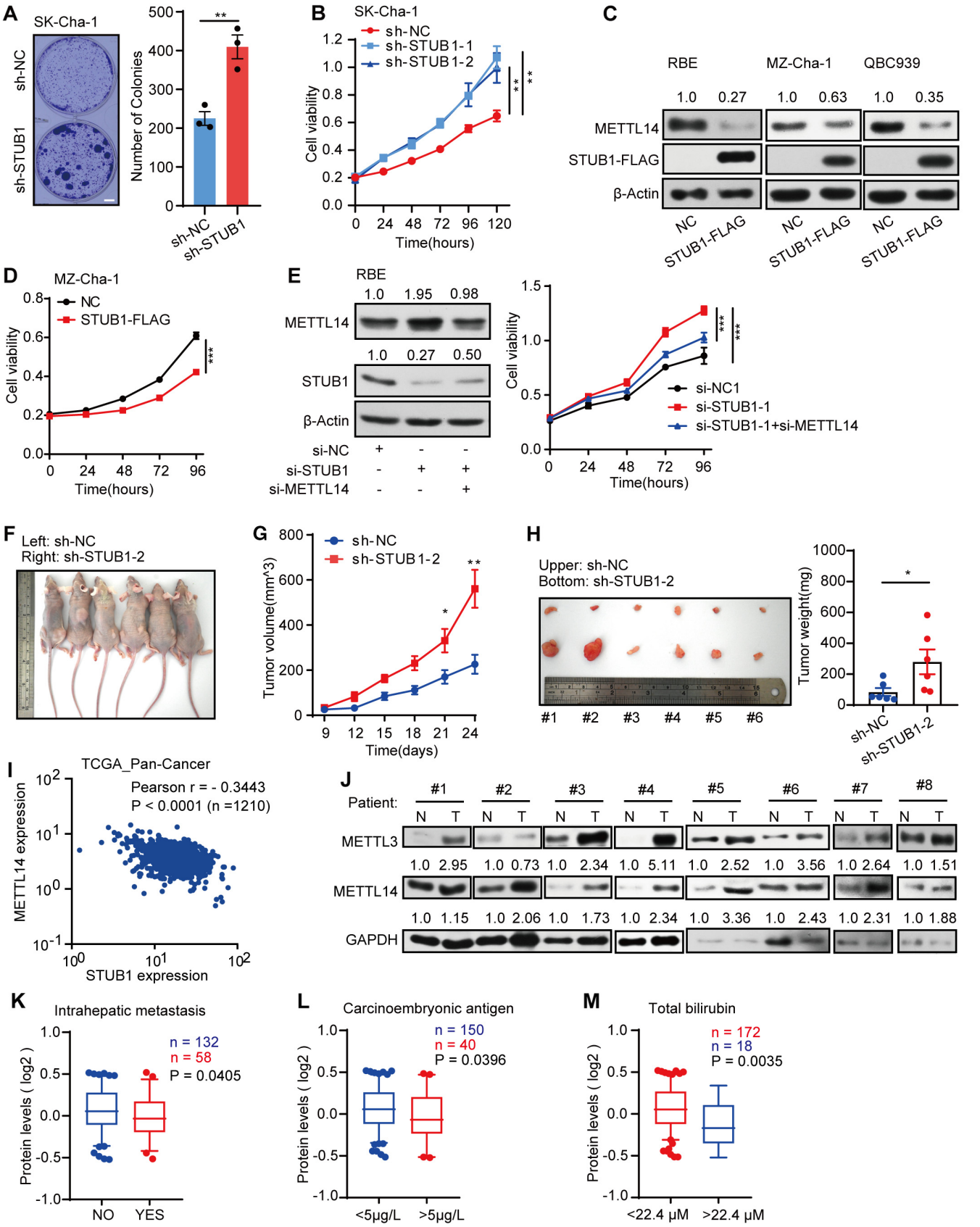
A
SK-Cha-1
sh-NC
sh-STUB1
Number of Colonies
sh-NC
sh-STUB1
B
SK-Cha-1
sh-NC
sh-STUB1-1
sh-STUB1-2
Cell viability
Time(hours)
C
RBE
MZ-Cha-1
QBC939
METTL14
STUB1-FLAG
β-Actin
NC
STUB1-FLAG
D
MZ-Cha-1
NC
STUB1-FLAG
Cell viability
Time(hours)
E
RBE
METTL14
STUB1
β-Actin
si-NC
si-STUB1
si-METTL14
Cell viability
si-NC1
si-STUB1-1
si-STUB1-1+si-METTL14
Time(hours)
F
Left: sh-NC
Right: sh-STUB1-2
G
sh-NC
sh-STUB1-2
Tumor volume(mm^3)
Time(days)
H
Upper: sh-NC
Bottom: sh-STUB1-2
Tumor weight(mg)
sh-NC
sh-STUB1-2
I
TCGA_Pan-Cancer
Pearson r = - 0.3443
P < 0.0001 (n =1210)
METTL14 expression
STUB1 expression
J
Patient:
METTL3
METTL14
GAPDH
K
Intrahepatic metastasis
n = 132
n = 58
P = 0.0405
Protein levels (log2)
NO
YES
L
Carcinoembryonic antigen
n = 150
n = 40
P = 0.0396
Protein levels (log2)
<5μg/L
>5μg/L
M
Total bilirubin
n = 172
n = 18
P = 0.0035
Protein levels (log2)
<22.4 μM
>22.4 μM

Figure EV5.